Energy Harvesting and Sensing with Embedded Piezoelectric Ceramics in Knee Implants

Mohsen Safaei, *Student Member, IEEE,* R. Michael Meneghini, and Steven R. Anton

Abstract — The knee replacement is one of the most common orthopedic surgical interventions in the United States; however, recent studies have shown up to 20% of patients are dissatisfied with the outcome. One of the key issues to improving these operations is a better understanding of the ligamentous balance during and after surgery. The goal of this work is to investigate the feasibility of embedding piezoelectric transducers in the polyethylene bearing of a total knee replacement to act as self-powered sensors to aid in the alignment and balance of the knee replacement by providing intra- and postoperative feedback to the surgeon. A model consisting of a polyethylene disc with a single embedded piezoelectric ceramic transducer is investigated as a basis for future work. A modeling framework is developed including a biomechanical model of the knee joint, a finite element model of the knee bearing with encapsulated transducer, and an electromechanical model of the piezoelectric transducer. Model predictions show that a peak voltage of 2.3 V with a load resistance of 1.01 $M\Omega$ can be obtained from a single embedded piezoelectric stack, and an average power of 12 μW can be obtained from a knee bearing with four embedded piezoelectric transducers. Uniaxial compression testing is also performed on a fabricated sample for model validation. The results found in this work show promising potential of embedded piezoelectric transducers to be utilized for autonomous, self-powered in vivo knee implant force sensors.

Index Terms — Energy harvesting, orthopedic implant, piezoelectric sensing, self-powered sensors, total knee replacement

I. INTRODUCTION

Each year, over 620,000 patients receive total knee replacements (TKRs) in the US [1], however, a recent study shows that only eighty percent of patients are satisfied with their function and level of pain after surgery [2]. A major complication of TKRs is improper ligamentous balance which can lead to accelerated loosening, instability and wear of the articular surfaces, reduced range of motion, and osteolysis. Sharkey et al. [3] reported that infection, loosening, and instability are the three main causes of knee implant failure. Current surgical practices for the balance of ligamentous forces rely heavily on the surgeon's experience and their interpretation of the tactile "feel" of a balanced knee [4, 5]. The lack of

quantitative measures for intraoperative balancing presents a need to measure tibiofemoral forces *in vivo* to develop improved surgical procedures and implant designs [6]. For reference, a schematic of a standard knee implant is illustrated in Fig. 1 showing the femoral component, tibial tray, and ultra high molecular weight (UHMW) polyethylene bearing.

The use of sensors for intra- and postoperative measurement has attracted much interest in the field of biomedical research in recent years, especially in the field of orthopedics. Intraoperative sensory systems are currently commercially available for use in total knee replacement surgeries, however, they are utilized for intraoperative data acquisition and must be removed prior to the conclusion of the surgery, as they are not capable of in vivo survival [6-8]. These intraoperative sensors, therefore, cannot provide any postoperative measurements. Several research groups have investigated the development of embedded sensors for intra- and postoperative measurement of tibiofemoral forces. Early works dating back to the mid-90's first explored the use of load cells or strain gages for measurement of forces and moments in TKRs [9-12]. The first sensor-embedded TKR to be implanted in a patient to collect in vivo data was presented by D'Lima et al. in 2006 and consisted of four embedded load cells and a microtransmitter for wireless communication [10]. The limitation of early designs is that they require an external power source, which is achieved via inductive coupling through an obtrusive coil system placed around the patient's knee. Since the physical movement of the patient's knee can be obstructed due to this external fixturing, the collected data may not represent the uninhibited joint motion.

The optimum data collection method for in vivo force measurement would allow for acquisition during surgery as well
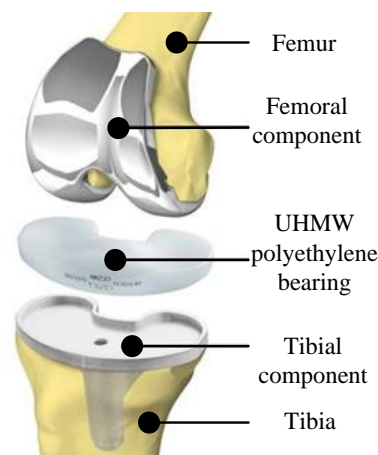
Fig. 1. Schematic of a total knee replacement implant.

as postoperatively during normal daily activities without disturbing the patient. To this end, a few recent studies have investigated the use of piezoelectric transducers to sense knee loads as well as to harvest compressive knee forces in order to create energy to power the embedded sensor system [13-18]. In one of the most recent works, Almouahed et al. [15] presented a design in which four low profile piezoelectric transducers were placed between the tibial tray and polyethylene bearing to measure knee forces as well as center of pressure. Results showed successful identification of center of pressure as well as the ability to harvest around 5 mW of raw power under simulated uniaxial knee loading. The drawback, however, of existing self-powered approaches is that the traditional implant design is modified in order to accommodate the energy harvesting and sensing components which requires modification of surgical techniques and presents challenges for the adoption of these designs into everyday practice. A more ideal scenario would be to embed the sensors in the polyethylene bearing in order to allow traditional and FDA-approved tibial components to be used as well as to locate the sensing device in the closest proximity of the contact point and force to optimize accuracy.

This paper aims to show, through a combined numerical and experimental approach, that piezoelectric ceramic transducers can be embedded into the polyethylene bearing of a TKR to act as self-powered sensors in order to improve the alignment and balance of the knee replacement by providing both intraoperative and postoperative feedback. Specifically, this work focuses on the sensing and energy harvesting performance of embedded piezoelectrics and builds upon the author's previous work [19]. A simplistic bearing design consisting of a single piezoelectric transducer placed in the center of a cylindrical disc of polyethylene is adopted in this work to allow investigation of the coupled physics of embedded piezoelectrics. Biomechanical modeling, finite element analysis, and electromechanical modeling are used to develop a comprehensive modeling framework capable of predicting the performance of an embedded piezoelectric device. Based on the modeling framework, simulations are performed for embedded monolithic and stack piezoelectric configurations. Fabrication of several simplified bearings is accompanied by uniaxial compression testing to validate the models. The overall goal of this work is to show that the electricity generated by a piezoelectric element integrated into a knee replacement bearing under normal walking conditions is sufficient to be measured by a typical low power circuit (that can also be embedded in the bearing), as well as to power the embedded circuit.

II. CONCEPTUAL DESIGN

The conceptual design envisioned for the future of this work consists of a UHMW TKR bearing with multiple (four or more) embedded piezoelectric transducers, as show in Fig. 2 (a). Multiple embedded piezoelectric elements are potentially capable of providing the ability to sense and transmit the magnitude and location of the applied compartmental forces on the UHMW bearing surface through an integrated circuit including signal conditioning, data storage, and data transmission components. In addition, the envisioned embedded piezoelectric transducer system is capable of harvesting and storing energy to power the aforementioned encapsulated electronics using separate power harvesting circuitry. The abovementioned circuitries will be embedded along with the piezoelectric transducers inside the knee bearing. The final instrumented implant eventually works in two distinct modes; energy harvesting mode and sensing mode. In energy harvesting mode, the sensing circuitry is on standby to decrease the power consumption, and the device harvests and stores the energy from knee motion during daily activities. On the other hand, the system switches to sensing mode for a short period of time and starts to collect, process, and transmit data from the knee according to a predefined procedure by the doctor using the stored power. The data obtained from the knee joint in terms of axial forces and the location of contact points represents the alignment and health of the joint, which can be used by surgeons, physical therapists, and medical device manufacturers to help improve surgical procedures and implant designs.

In this work, a simplified bearing geometry is adopted in order to allow investigation of the feasibility of the conceptual design in terms of both sensing and energy harvesting, as well as fabrication of prototype devices and subsequent uniaxial compression testing. Specifically, a cylindrical disc of UHMW with a smaller cylindrical piezoelectric ceramic element embedded within the polyethylene at the geometric center is used, as shown in Fig. 2 (b). It should be noted that UHMW is the most commonly used material in orthopedic implant bearings thanks to its low coefficient of friction, good wear resistance, and biocompatibility [20]. PZT-5A, a lead zirconate titanate piezoelectric material, is used in this work since it is a common material widely used in the piezoelectric energy harvesting and sensing community, and is readily available from various manufacturers [21]. The UHMW disc has a diameter of 45 mm and a thickness of 8 mm. These dimensions are chosen to simulate the approximate size of a TKR bearing. The piezoelectric transducer has a diameter of 8 mm and a thickness of 3 mm, which allows for eventual placement of multiple, spatially distributed transducers within the bearing. A cylindrical pocket of 8 mm diameter and 3 mm depth is removed from the UHMW disc to allow the piezoelectric transducer to fit perfectly within the disc. These dimensions are defined in this work as the *reference geometry* of the system. The material properties and geometry of the UHMW and piezoelectric transducer are given
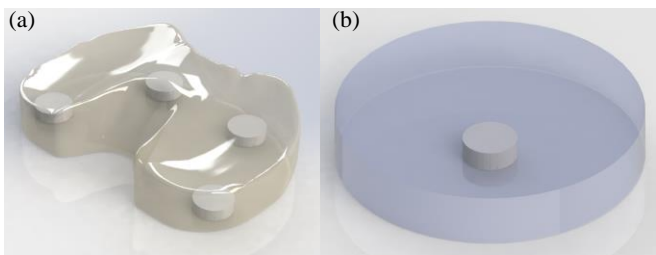

Fig. 2. Schematic of (a) conceptual UHMW bearing with multiple embedded piezoelectric transducers and (b) simplified UHMW bearing investigated in this work with a single embedded piezoelectric transducer.

Geometric Properties	UHMW Bearing	PZT-5A Piezoelectric	Material Properties	UHMW Bearing	PZT-5A Piezoelectric
Diameter [mm]	45	8	Young's modulus [GPa]	0.83	54
Thickness [mm]	8	3	Poisson's Ratio	0.42	0.35
			Density [kg/m^3]	950	7600
			Piezoelectric Constant, d_{33} [pC/N]	——	400
			Relative Permittivity, $\varepsilon_{33}^T / \varepsilon_0$	——	1900

in TABLE I. The material properties of UHMW are taken from the UHMW biomaterials handbook [22], and the properties of PZT-5A (APC 850) are taken from the manufacturer (APC International, Ltd.) specifications [23].

III. MODELING

A three-phase modeling framework is developed in this work in order to predict the behavior of a piezoelectric transducer embedded in a polyethylene TKR bearing. In the first phase, biomechanical modeling is performed using OpenSim modeling software to predict the force loading experienced by the knee during normal walking conditions. In the second phase, finite element analysis is performed in ANSYS software in which a simplistic bearing with embedded piezoelectric transducer is subjected to the predicted knee loads from the first phase in order to predict the percentage of axial load that is transferred through the polyethylene bearing to the embedded piezoelectric. Lastly, the third phase involves electromechanical modeling using MATLAB software to predict the voltage and power generation of the piezoelectric transducer given the loads calculated in the second phase by finite element analysis. Each modeling phase is described in detail in the following sections, and the modeling framework is then applied in order to simulate the output of the system in terms of generated voltage and power from embedded monolithic (to allow experimental validation) and stack transducers.

A. BIOMECHANICAL MODELING

In order to accurately predict the electrical output of a piezoelectric element embedded in a polyethylene knee replacement bearing, it is necessary to first determine the force experienced by the knee joint under normal walking gait. Many studies have focused on the development of such a force profile throughout the past several decades [24, 25]. While valuable information about the force behavior of the knee joint has been provided by these studies, none of these models have produced predictions that closely match data collected from instrumented knees.

In this work, OpenSim, an open source biomechanical modeling software [26], is used to simulate the tibiofemoral force profile experienced in normal walking gait that is used throughout this research. The software combines experimental kinematic data with numerical models of human anatomy and can be used to predict joint reaction forces. The software utilizes several input parameters, such as kinematics of gait, force actuator data for ligaments, and external loads on the foot, in a joint analysis tool to calculate the joint reaction forces on the musculoskeletal model.

The axial force profile developed in OpenSim is shown in Fig. 3. It should be noted that the independent variable used in the figure is gait percentage which maps linearly to time. The timespan of the data shown in the figure is 1.2 sec. As shown in the figure, the load profile has two separate peaks. The first peak is associated with the impact loading experienced by the knee joint when the heel strikes the ground. The second peak corresponds to the maximum force experienced by the knee as weight transfers from one foot to the other. Furthermore, the peak force is roughly 3.4 times bodyweight, which agrees well with peak values suggested in the literature of around 2.5-3 times body weight [27, 28]. It should be noted that the model used in the present simulation predicts the knee force for a 165.7 lb and 70.8 in healthy male under normal walking gait, and can be different for individuals with different age, weight, height, and gait pattern. This load profile provides a reasonable approximation of tibiofemoral force for a general case and will be used throughout this study.

B. FINITE ELEMENT MODELING

With the tibiofemoral load profile determined, it is possible to utilize finite element (FE) analysis to predict the amount of force that is transferred through the polyethylene bearing to an embedded piezoelectric transducer. In this study, a finite element
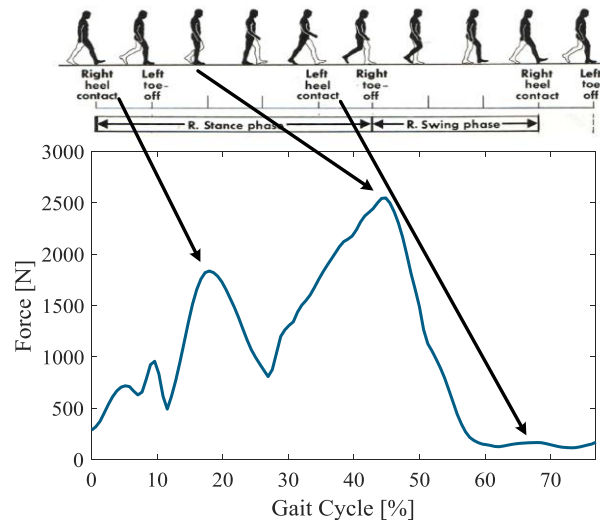

Fig. 3. Axial force profile developed in OpenSim for a 165.7 lb (75 kg) male who is 70.8 in (180 cm) tall under normal walking gait.
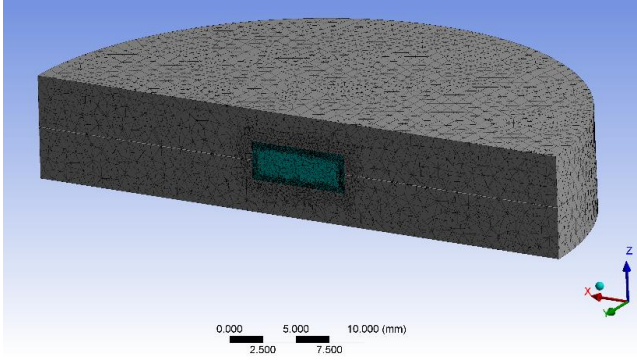
Fig. 4. Cross-sectional view of finite element model showing embedded piezoelectric and mesh detail.

model of the polyethylene knee bearing with an embedded piezoelectric transducer is created in ANSYS. A cross-sectional view of the finite element model is given in Fig. 4. The model consists of SOLID187, CONTA174, and TARGE174 (for contact surfaces) elements automatically selected and placed by the software, and contains 622,649 nodes and 431,944 elements. The element size for PZT and UHMW are 0.3 mm and 0.8 mm with a maximum aspect ratio of 7.5, which are finely refined on the corners and on the contact surfaces. A mesh refinement study was conducted to ensure that the model predictions converged. It should be noted that piezoelectricity is not considered in the finite element model and is addressed separately using an electromechanical model, therefore, the piezoelectric transducer is modeled as a passive element. The boundary conditions between the embedded piezoelectric and the UHMW disc are defined to be frictional with a friction coefficient of 0.12 [22, 29]. The bottom face of the UHMW has a frictionless support applied. This is intended to replicate the unconstrained lateral expansion of the bottom face when the UHMW sample is loaded in compression. The external force is applied in component form to act solely in the z-direction (refer to Fig. 4) in order to duplicate the uniaxial load case that is to be replicated experimentally. Again, these forces are derived from the load profile that was generated using OpenSim. A transient analysis is performed with an initial timestep of 0.01 sec and 120 steps. Force and displacement convergence are achieved for all the steps with 206 cumulative number of iterations.

C. ELECTROMECHANICAL MODELING

The electromechanical behavior of piezoelectric materials is well described in the IEEE Standard on Piezoelectricity [30]. The governing equation for an N-layer piezoelectric stack under uniform compressive loading (as utilized in this work), assuming that the electrodes of each piezoelectric layer in the stack are connected in parallel to a single resistor, is given by

$$C_p^{eff} \frac{dv(t)}{dt} + \frac{v(t)}{R} = d_{33}^{eff} \dot{F}(t), \qquad (1)$$

where C_p^{eff} is the effective piezoelectric capacitance, $v(t)$ is the voltage output across the resistor, R, d_{33}^{eff} is the effective

piezoelectric constant, and $F(t)$ is the compressive force applied to the piezoelectric stack. The effective piezoelectric capacitance can be stated as

$$C_p^{eff} = \frac{N \varepsilon_{33}^T A}{h}, \qquad (2)$$

where ε_{33}^T is the dielectric constant, A is the surface area, and h is the thickness of a single layer. The effective piezoelectric constant can be expressed as

$$d_{33}^{eff} = N d_{33}.$$

where d_{33} is the piezoelectric strain constant. It is necessary to note that, based on Eq. (1), generated voltage and applied force on the piezoelectric transducer (sensed force) are correlated. Therefore, results presented in this work in terms of voltage or force represent the sensing performance of the system similarly. Furthermore, the average power, P_{avg}, can be found by

$$P_{avg} = \frac{1}{T} \int_0^T \frac{v^2(t)}{R} dt, \qquad (3)$$

where T is the time span for the simulation.

It should be noted that the governing expression given in Eq. (1) for the voltage generated by a piezoelectric disk under an input force is first-order. This equation, in contrast to common resonant-based energy harvesting models, therefore, is valid for excitation frequencies significantly below the resonance frequency of the device. In this regime, the harvester exhibits first-order dynamics; such is the case in this work.

MATLAB software is used in this work to numerically simulate the piezoelectric output. Again, the input force used in the MATLAB simulation is derived by applying the OpenSim force profile as the input to the finite element model and determining the percentage of force that is transferred through the UHMW to the piezoelectric transducer.

D. MODELING RESULTS

Using the modeling framework described in the previous sections, the electromechanical behavior of the sample illustrated in Fig. 4 is obtained. Initially, a monolithic piezoelectric transducer is chosen based on the availability of transducers obtained to experimentally validate the model. Fig.
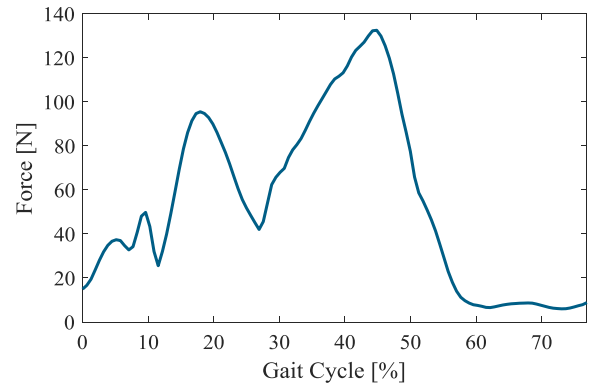

Fig. 5. Transferred force to the embedded PZT transducer obtained from FE.

5 shows the force profile transferred to the embedded PZT transducer in the UHMW disk obtained from FE analysis. The ratio of the force applied to the PZT to the total force applied to the bearing (Fig. 3) is about 5%. This force profile is utilized in MATLAB to develop the voltage signal generated by the PZT element. Fig. 6 shows the generated (a) voltage and (b) average power using the reference geometry, and for various load resistances. When simulating the generated voltage, the resistive loads are chosen from 99.7 $k\Omega$ to 1.01 $M\Omega$ to represent a realistic range of loads for piezoelectric energy harvesting and sensing (specific values are selected to match those used in the experimental testing, as described later). It can be seen that the output voltage of the PZT transducer increases with resistive load, as expected, and for a 1.01 $M\Omega$ resistor, a peak absolute voltage of around 0.5 V is obtained. When simulating the average output power of the system, a much broader range of load resistances is used to capture the optimal load resistance. From the results, it can be seen that a maximum of 3 μW is generated for a 428 $M\Omega$ optimal load resistance. The behaviors shown in Fig. 6 are expected and well known for piezoelectric transduction.

The large optimal resistive load for maximum harvested power is a result of the monolithic nature of the piezoelectric transducer. It should be noted that the purpose of the model presented here for a monolithic piezoelectric element is to allow experimental validation (presented in the next section). Utilization of a piezoelectric stack transducer, on the other hand, can result in a significant reduction in the optimal load resistance to a more reasonable level due to the increase in capacitance as a result of the stack configuration [31]. Furthermore, the output voltage of the PZT element can be optimized (in this case, increased for improved sensing and energy harvesting performance) by using a specific stack configuration whereby the individual layers are wired in parallel.

In order to predict the performance improvement when utilizing a stack configuration, the model is updated to include a piezoelectric stack and simulations are performed to consider sensing and energy harvesting performance. As described previously, the envisioned embedded sensing system will consist of separate circuitry for load sensing and for energy harvesting (each with independent effective load resistance applied to the piezoelectric transducer). First, considering the sensing performance, Fig. 7 (a) illustrates the variation of maximum voltage generated from an embedded piezoelectric stack under a load resistance of 1.01 $M\Omega$ (1 $M\Omega$ is a common input impedance for analog-to-digital converters, and previous simulations have been performed at 1.01 $M\Omega$, therefore, this is chosen here for comparison purposes) for various number of piezoelectric layers up to 50 layers. Note, the overall thickness of the PZT remains constant while the number of layers is varied in the simulation. Input voltages in the range of 1 to 2.5 V have been reported for low power sensing and data transmitting circuits for biomedical applications [32, 33], therefore, the simulation results show that a piezoelectric stack with at least ~5 layers can provide adequate voltage for sensing purposes. Next, the energy harvesting performance can be considered. As mentioned previously, a stack geometry can yield more reasonable matched resistive load for maximum attainable power as compared to a monolithic transducer. Fig. 7 (b) shows the optimal resistive load to obtain maximum power as well as the peak generated voltage under the corresponding optimal resistive load for a piezoelectric stack with different number of layers up to 50 layers. It has been reported that impedances from 10 $k\Omega$ to 300 $k\Omega$ have been applied in piezoelectric based energy harvesting systems for different applications [34, 35]. Moreover, an input voltage around 1 V is shown to be adequate for low power implantable energy harvesting circuits for biomedical applications [36]. Considering the desired impedance and input voltage range, a piezoelectric stack with 40 to 50 layers can provide adequate voltage and matched impedance for energy harvesting electronics. In conclusion, based on the range of number of layers for sensing and energy harvesting performance, a piezoelectric stack with 40 layers and with a matched resistive load of 263 $k\Omega$ is chosen here to be compared with the monolithic case. The applied load, boundary conditions, transducer material, and overall geometry are identical to those used in the former analysis for a monolithic piezoelectric.
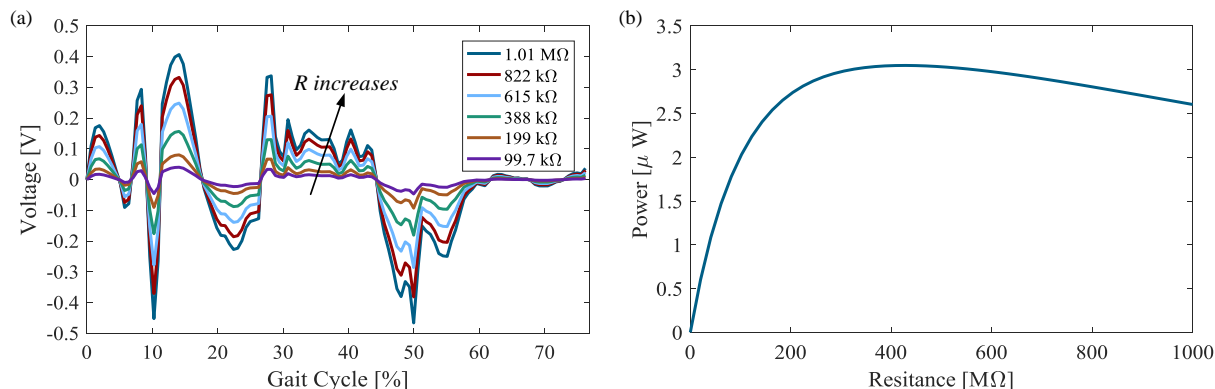

Fig. 6. Simulation results for uniaxially loaded embedded monolithic piezoelectric including (a) output voltage vs. gait cycle and (b) average output power vs. load resistance.
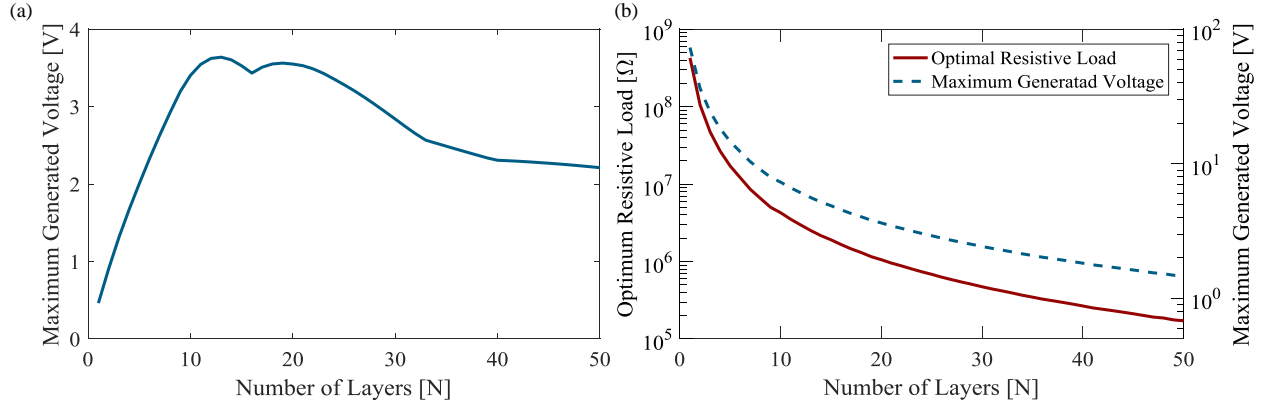
Fig. 7. (a) Variation of peak generated voltage from piezoelectric stack for different number of piezoelectric layers under 1.01 $M\Omega$ resistive load; (b) variation of optimal resistive load to obtain maximum average power and the peak generated voltage under optimum resistive load for various number of piezoelectric layers.

Fig. 8 shows the generated (a) voltage and (b) average power for a UHMW disc with embedded 40-layer PZT-5A stack. Compared to the monolithic piezoelectric (presented previously in Fig. 6), a remarkable increase in output voltage of the system for sensing purposes can be observed (a peak absolute voltage of 2.3 V for a stack vs 0.5 V for a monolithic transducer for a 1.01 $M\Omega$ load resistor). Furthermore, simulation results also show that the average output power of 3 μW can be obtained for an optimum resistor of 263 $k\Omega$ for the stack compared to 428 $M\Omega$ for the monolithic transducer, which is much more reasonable for piezoelectric energy harvesting circuitry. Note, the voltage vs. gait cycle profile exhibits differences between monolithic piezoelectrics (Fig. 6 (a)) and multilayer stacks (Fig. 8 (a)). This is due to the nonlinearity of the system parameters (capacitance and piezoelectric coupling terms) in Eq. (1), which dictate the time response of the system. Considering the conceptual design of an instrumented knee bearing system containing four embedded piezoelectric transducers (Fig. 2 (a)) under full knee load, an average power of 12 μW can be generated from the system during a single gait cycle. With regards to the power

required to sense and transmit knee loads, previous research has shown that a circuit designed for collection and processing of the data from force sensors embedded in knee implants (circuit contains a signal conditioner, microprocessor, power management circuit, and wireless transmitter) shows a power consumption as low as 140 μW [33]. The system explored in this work, therefore, provides promising potential to supply power to an integrated measurement circuit and allow operation on a duty cycle around 8.5%, while simultaneously sensing the forces applied to the UHMW bearing.

IV. EXPERIMENTAL VALIDATION

In order to verify the finite element and electromechanical models discussed in Sec. III-B and Sec. III-C, it is necessary to build a physical prototype and subject it to experimental testing in order to compare modeling predictions to experimental measurements. Details of the prototype bearing fabrication with embedded piezoelectric transducer, experimental compression testing, and comparisons between model predictions and experimental results are given in the following sections.
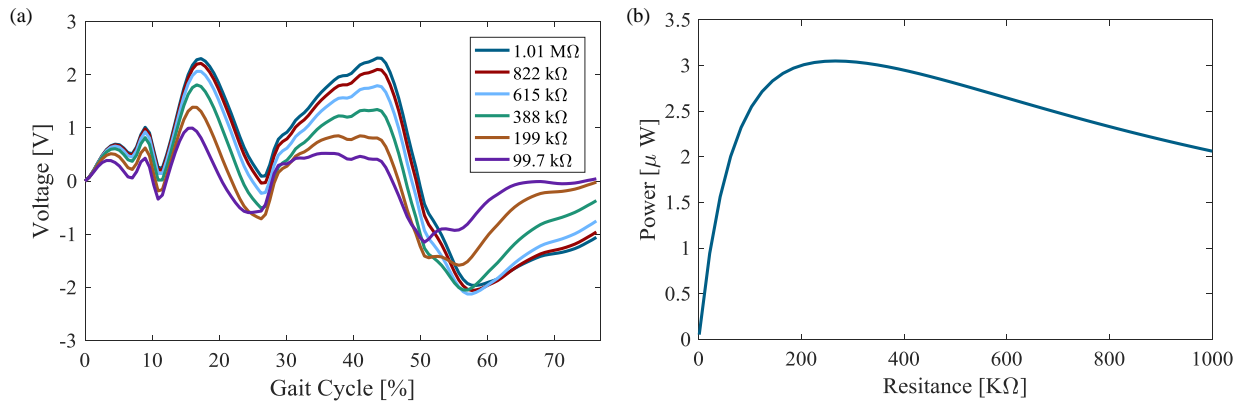

Fig. 8. Simulation results for uniaxially loaded embedded 40-layer piezoelectric stack including (a) output voltage vs. gait cycle and (b) average output power vs. load resistance.
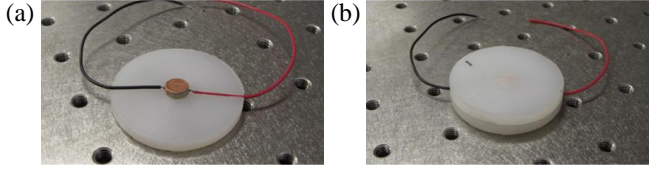
6

Fig. 9. Fabricated bearing showing (a) inserted piezoelectric and (b) fully assembled bearing.

A. *SAMPLE FABRICATION*

As discussed previously, a simplified bearing geometry is adopted in this work in order to allow for fabrication of prototype devices and subsequent uniaxial compression testing. The specimens created in this work consist of a disc of UHMW sectioned into upper and lower halves with recessed pockets for a smaller piezoelectric disc to be placed within the bearing. Photographs of the fabricated samples are given in Fig. 9. The geometric properties of the fabricated device match those utilized for the model and given previously in TABLE I. Due to availability, a monolithic PZT-5A piezoelectric element (APC 850) is used in the prototype device. The thickness mode natural frequency of the piezoelectric element is 680 kHz. The highest frequency contained in the input force profile is approximately 25 Hz. This is far below the resonance frequency of the piezoelectric element, which indicates that use of the first-order analytical expressions discussed in Sec. III-C is valid.

Fabrication of the prototype bearings is accomplished by first machining two 4 mm thick UHMW discs with a diameter of 45 mm. Each disc then has a 1.5 mm deep, 8 mm diameter area machined away to provide space for the piezoelectric element to be press fit into place. Next, two grooves are cut into each UHMW disc, 180 degrees offset from one another, extending outward from the embedded piezoelectric element to allow for electrical leads to run from the piezoelectric element to the measurement device. Leads are soldered onto the piezoelectric elements in a manner that allows the leads to exit the sides of the device. This allow the upper and lower surfaces to be free from leads or solder connections and sit flush against the UHMW. One lead is soldered onto an existing factory tab electrode that extends to the side of the piezoelectric element, and the other lead is soldered to a fabricated tab electrode created out of copper tape with conductive adhesive that is placed on the piezoelectric surface lacking a factory tab electrode and wrapped to the side of the device.

It should be noted that UHMW is a difficult material to machine and fabricating a sample with exact dimensions is challenging. Also, it is easily damaged by excessive heat or improper feed rate, so great care must be taken to control the machining environment [22]. Due to fabrication difficulties, machining inconsistencies will be experimentally investigated and presented later in this section. It should also be noted that an eventual self-powered knee sensor would contain all necessary electronics and electrical connections embedded within the bearing, however, the prototype in this work only contains an
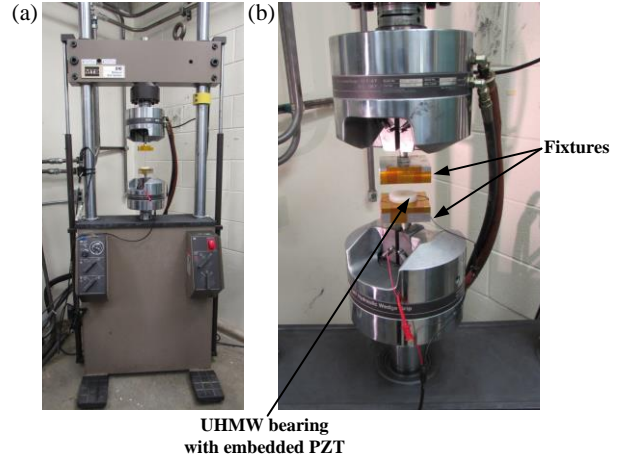

Fig. 10. Experimental compression test setup including (a) MTS 810 servo hydraulic load frame, (b) close-up view of prototype bearing inserted into compression fixturing.

embedded piezoelectric device which requires electrical connections to external equipment.

B. *COMPRESSION TESTING SETUP*

An MTS 810 servo-hydraulic load frame is employed in order to conduct uniaxial compression testing, as illustrated in Fig. 10. The force profile predicted by OpenSim (shown previously in Fig. 3) is used as the input to the load frame. PID control parameters are tuned in the load frame controller software in an attempt to achieve the desired profile. Due to mechanical limitations of the machine, accurate replication of the desired load profile is impossible, therefore, some discrepancies will be present. The desired load profile and the load profile achieved by the MTS load frame are compared and plotted in Fig. 11 (note, both time and gait percentage are shown for clarity). In this figure, it can be seen that the MTS load frame tracks the desired load profile well, however, there are some areas where the force changes at a higher rate than the load frame is able to follow. It is expected that experimental data in these regions will have slight discrepancies in the voltage produced when compared to model predictions.

Compression tests are conducted in order to determine the voltage output across a series of load resistances, ranging from ~100 $k\Omega$ to ~1 $M\Omega$ in order to validate the finite element and electromechanical models. Using a National Instruments NI-9215 data acquisition card, the voltage output of the PZT across a load resistance (achieved using carbon film resistors) is acquired during compression testing and the applied force profile is recorded directly using the MTS load frame software; both at a rate of 1024 Hz.

C. *COMPARISON OF MODELING AND EXPERIMENTAL RESULTS*

Preliminary experimental measurements showed a low signal-to-noise ratio which prompted further investigation before comparison of experimental measurements with model predictions. Digital filtering was performed in an effort to reduce unwanted noise in the measurement signal, which resulted in

improved measurements, however, signal levels were still much lower than expected. Upon further investigation, it was observed that the fabricated sample geometry deviated from the target reference geometry. In fact, the most difficult part of the sample fabrication is removing material to form the pockets where the PZTs are placed in the UHMW discs. Measured dimensions from several fabricated samples show that the pocket depth exhibits some deviation from the reference dimension. After experimentation with several fabricated samples, the chosen sample had a total pocket depth of 2.92 mm whereas the reference pocket depth was 3 mm. This difference resulted in producing a gap of 0.08 mm between the UHMW bearing halves after installation of the PZT transducer. Initial testing and modeling for this sample showed a higher generated voltage and greater signal-to-noise ratio compared to the reference geometry (due to higher force transferred to the PZT), thereby providing a more suitable platform to evaluate the modeling and experimental results. Due to the higher electromechanical performance of this sample compared to the reference geometry, it was considered the ideal geometry in this study.

Results of both simulation and experimental testing are presented in Fig. 12. Using the modeling framework described in Sec. III, simulation of the voltage generated across a range of load resistances (considering the geometry discussed above with a 0.08 mm gap between the two UHMW halves) subject to the predicted tibiofemoral force are given in Fig. 12(a). The geometry and material properties provided in TABLE I are used in the simulations. As expected, the predictions show modulating voltage output corresponding to the applied load profile and monotonically increasing voltages with increasing load resistance.

Experimentally measured voltage histories are given in Fig. 12(b). The same set of load resistances used in the simulations are also used in the experiments for comparison purposes. Comparing the modeling and experimental results, it can be seen that the experimental data has several small fluctuations that do not appear in the simulation results.

This phenomenon can be attributed to the low amplitude, high frequency fluctuations in the force profile generated by the closed-loop control electronics of the load frame (not shown in
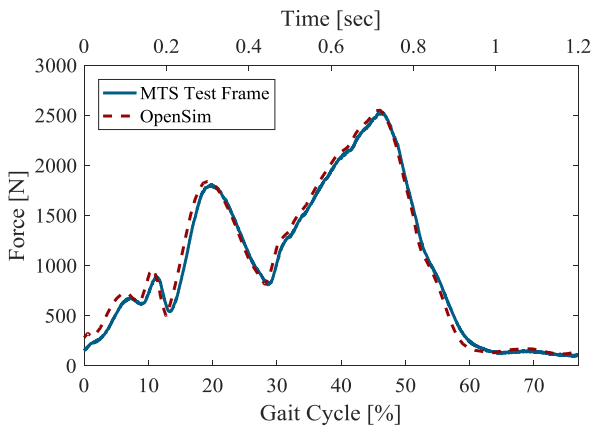
Fig. 11 due to relatively low sampling rate of the load frame). In addition, the measured force applied to the piezoelectric transducer is calculated using the experimentally captured voltage signal for the 1 $M\Omega$ load resistance shown in Fig. 12 (b) along with Eq. (1). The measured force profile is compared to the profile obtained from FE analysis in Fig. 13. The voltage signal and force results show that the model and experiment match quite well with only small errors that can be partially attributed to the nonlinear behavior of UHMW [37] and partially attributed to geometric simplifications and assumed boundary conditions in the finite element model. Overall, the model predictions match the experimental measurements well, thereby validating the modeling framework utilized in this work. Furthermore, it should be noted that these levels are satisfactory for recording with standard analog-to-digital converters that can be employed in an embedded knee load sensing circuit.

D. FABRICATION VARIATION

After the initial data set was recorded, additional samples were fabricated to have a larger sample size for more robust results. Upon preliminary testing, it quickly became clear that slight changes in the machining of the pockets in the UHMW discs had drastic effects on the voltage output. To determine the significance of the effect of pocket depth, additional compression tests were run with four different UHMW disc assemblies with encapsulated piezoelectric elements. The piezoelectric element used in this study has a height of 3 mm.

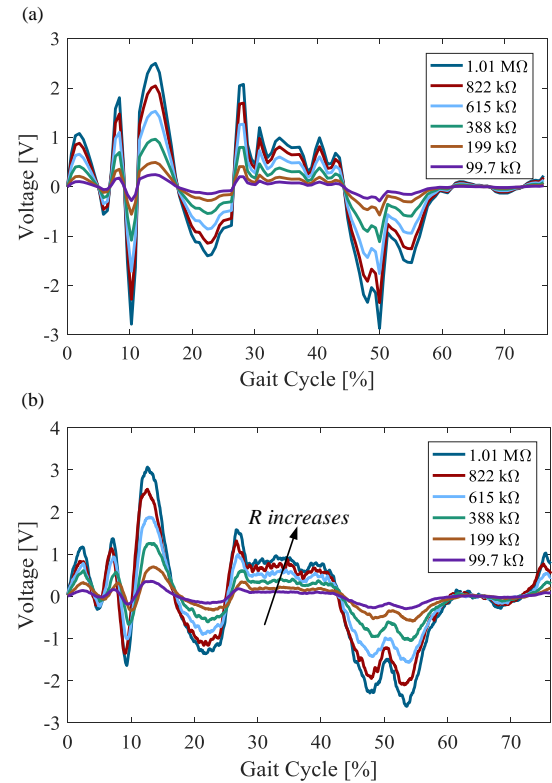Fig. 12. Generated voltage for uniaxially loaded embedded piezoelectric element in UHMW with 80 μm gap obtained from (a) simulation and (b) experiment.

Fig. 11. Comparison of load profile generated by OpenSim and achieved by MTS test frame.
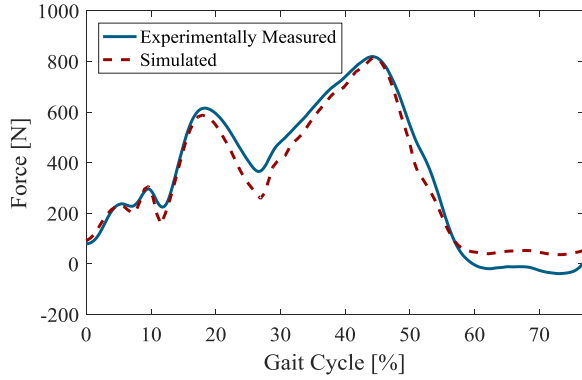
Fig. 13. Comparison of force profile on the piezoelectric measured by PZT (experiment) and obtained from simulation.

The ideal height for the machined UHMW pocket is considered 2.92 mm to ensure a preexisting gap and adequate contact, as discussed previously in Sec. IV-C. A load resistance of 1.01 $M\Omega$ was used for all testing. The results of these tests can be seen in Fig. 14. The total pocket depth for each UHMW sample can be seen in TABLE II. It is necessary to note that the test results presented in the previous sections belong to UHMW Sample #1. The depth of the pocket machined in the UHMW sample clearly has a remarkable effect on the voltage output. If the pocket depth is too shallow, as seen in Fig. 14 for UHMW Sample #3, the UHMW does not absorb the anticipated percentage of the load as the load path travels primarily through the piezoelectric element since the top portion of the UHMW does not completely contact the lower portion of the UHMW (a gap remains even after application of load). While this results in higher voltage generation, it also results in larger stress concentrations developing within the bearing, which could cause premature failure. Conversely, if the pocket depth is close to the reference geometry, as seen in Fig. 14 for UHMW Sample #4, the UHMW absorbs a higher portion of the load as the top and bottom pieces of UHMW apply little compressive force to the embedded transducer (the gap closes and the UHMW absorbs much of the load), and the voltage output suffers. This figure clearly shows that very tight machining tolerances must be observed in order to achieve predictable output.

V. CONCLUSION

This research investigates the development of self-powered total knee replacement sensors by embedding piezoelectric ceramic transducers into the UHMW tibial bearing of a total knee replacement unit to measure forces in the knee intraoperatively and postoperatively, as well as to harvest energy

TABLE II. POCKET DEPTH OF UHMW SAMPLES.

UHMW Sample #	Pocket Depth (mm)
1	2.92
2	2.88
3	2.90
4	2.96

to power embedded data acquisition and transmission circuitry. In this study, a simplistic design consisting of a single piezoelectric transducer embedded in a UHMW disc is studied. It should be noted, however, that the envisioned fully-functional conceptual design will contain four or more transducers embedded in the polyethylene bearing for accurate sensing of force amplitude and location.

First, a three phase modeling framework consisting of biomechanical modeling, finite element modeling, and electromechanical modeling is established to simulate and predict the electromechanical performance of the simplistic system for an average sized man under normal walking gait. Simulation results show that a monolithic piezoelectric transducer generates 0.5 V peak under a 1.01 $M\Omega$ resistor and 3 μW of average power at a relatively high matched load resistance of 428 $M\Omega$. In order to reduce the matched load resistance, a stack transducer with the same overall dimensions is employed to re-simulate the performance of the system. As a result of a parametric study on the number of layers of the piezoelectric stack, a 40-layer stack is chosen. Modeling results show that a peak voltage of 2.3 V for a 1.01 $M\Omega$ load resistor and 3 μW of average power at a matched load resistance of 263 $k\Omega$ are generated. Furthermore, these results show that 12 μW of average power can be generated by a system containing four embedded stacks. Based on the literature, this power level is deemed sufficient to power a low power sensor for use in in vitro and in vivo data collection in TKR patients.

Next, several samples are fabricated for experimental model validation, each including two UHMW bearing halves and an encapsulated wired monolithic PZT ceramic. Due to fabrication difficulties, the pocket depth in the fabricated samples does not match the reference geometry. Considering this issue, a sample with 80 μm shallower pocket in the UHMW bearing, which generates a gap between the two bearing halves, is chosen for analysis.

Results obtained from uniaxial compression testing for embedded monolithic PZT-5A piezoelectric samples show good agreement with simulation results, thus validating the modeling framework developed in this work. Finally, the consistency of the fabricated samples is investigated by compression testing of
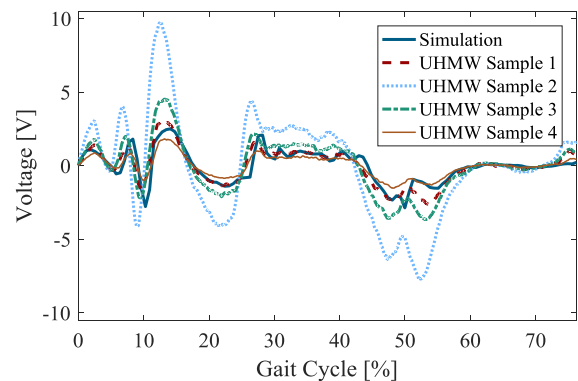

Fig. 14. Voltage output data for 4 UHMW samples with embedded piezoelectric element.

four samples. Testing results show that the depth of the PZT pocket in the UHMW bearing has a remarkable effect on the electromechanical output of the system. Overall, the results presented in this work show promise for embedded piezoelectric transducers to create autonomous, self-powered in vivo knee implant force sensors. Future studies are in progress to investigate the effects of different material and dimensional parameters on the performance of the proposed system, as well as the durability of the UHMW bearing and embedded sensor, in order to achieve an optimized design of the instrumented knee implant. Furthermore, the biocompatibility of the embedded sensory system will be investigated through exploration of biocompatible transducer packages such as PICMA transducers (PI Ceramic GmbH) and encapsulation in biocompatible compounds such as PDMS.

REFERENCES

[1] A. M. Weinstein, B. N. Rome, W. M. Reichmann, J. E. Collins, S. A. Burbine, T. S. Thornhill, *et al.*, "Estimating the burden of total knee replacement in the United States," *Journal of bone & Joint Surgery,* vol. 95, pp. 385-392, 2013.

[2] R. Bourne, B. Chesworth, A. Davis, N. Mahomed, and K. J. Charron, "Patient Satisfaction after Total Knee Arthroplasty: Who is Satisfied and Who is Not?," *Clinical Orthopaedics and Related Research,* vol. 468, pp. 57-63, 2010.

[3] P. F. Sharkey, P. M. Lichstein, C. Shen, A. T. Tokarski, and J. Parvizi, "Why are total knee arthroplasties failing today—has anything changed after 10 years?," *The Journal of arthroplasty,* vol. 29, pp. 1774-1778, 2014.

[4] J. Bellemans, H. Vandenneucker, J. Van Lauwe, and J. Victor, "A New Surgical Technique for Medial Collateral Ligament Balancing," *The Journal of Arthroplasty,* vol. 25, pp. 1151-1156, 2010.

[5] K. Tanaka, H. Muratsu, K. Mizuno, R. Kuroda, S. Yoshiya, and M. Kurosaka, "Soft tissue balance measurement in anterior cruciate ligament-resected knee joint: cadaveric study as a model for cruciate-retaining total knee arthroplasty," *Journal of Orthopaedic Science,* vol. 12, pp. 149-153, 2007.

[6] R. M. Meneghini, M. M. Ziemba-Davis, L. R. Lovro, P. H. Ireland, and B. M. Damer, "Can Intraoperative Sensors Determine the "Target" Ligament Balance? Early Outcomes in Total Knee Arthroplasty," *The Journal of arthroplasty,* vol. 31, pp. 2181-2187, 2016.

[7] K. A. Gustke, G. J. Golladay, M. W. Roche, L. C. Elson, and C. R. Anderson, "A New Method for Defining Balance: Promising Short-Term Clinical Outcomes of Sensor-Guided TKA," *The Journal of Arthroplasty,* vol. 29, pp. 955-960, 2014.

[8] M. Roche, L. Elson, and C. Anderson, "Dynamic Soft Tissue Balancing in Total Knee Arthroplasty," *Orthopedic Clinics of North America,* vol. 45, pp. 157-165, 2014.

[9] D. D. D'Lima, S. Patil, N. Steklov, S. Chien, and C. W. Colwell, Jr., "In vivo knee moments and shear after total knee arthroplasty," *Journal of Biomechanics,* vol. 40, pp. S11-S17, 2007.

[10] D. D. D'Lima, S. Patil, N. Steklov, J. E. Slamin, and C. W. Colwell Jr, "Tibial Forces Measured In Vivo After Total Knee Arthroplasty," *The Journal of Arthroplasty,* vol. 21, pp. 255-262, 2006.

[11] K. R. Kaufman, N. Kovacevic, S. E. Irby, and C. W. Colwell, "Instrumented implant for measuring tibiofemoral forces," *Journal of Biomechanics,* vol. 29, pp. 667-671, 1996.

[12] B. Kirking, J. Krevolin, C. Townsend, C. W. Colwell, Jr., and D. D. D'Lima, "A multiaxial force-sensing implantable tibial prosthesis," *Journal of Biomechanics,* vol. 39, pp. 1744-1751, 2006.

[13] S. Almouahed, M. Gouriou, C. Hamitouche, E. Stindel, and C. Roux, "Design and Evaluation of Instrumented Smart Knee Implant," *IEEE Transactions on Biomedical Engineering,* vol. 58, pp. 971-982, 2011.

[14] S. Almouahed, M. Gouriou, C. Hamitouche, E. Stindel, and C. Roux, "The Use of Piezoceramics As Electrical Energy Harvesters Within Instrumented Knee Implant During Walking," *IEEE/ASME Transactions on Mechatronics,* vol. 16, pp. 799-807, 2011.

[15] S. Almouahed, C. Hamitouche, E. Stindel, and C. Roux, "Optimization of an instrumented knee implant prototype according to in-vivo use requirements," in *2013 IEEE Point-of-Care Healthcare Technologies (PHT)*, 2013, pp. 5-8.

[16] S. R. Platt, S. Farritor, K. Garvin, and H. Haider, "The use of piezoelectric ceramics for electric power generation within orthopedic implants," *IEEE/ASME Transactions on Mechatronics,* vol. 10, pp. 455-461, 2005.

[17] S. R. Platt, S. Farritor, and H. Haider, "On low-frequency electric power generation with PZT ceramics," *IEEE/ASME Transactions on Mechatronics,* vol. 10, pp. 240-252, 2005.

[18] M. Safaei, R. M. Meneghini, and S. R. Anton, "Parametric analysis of electromechanical and fatigue performance of total knee replacement bearing with embedded piezoelectric transducers," *Smart Materials and Structures,* vol. 26, p. 094002, 2017.

[19] B. E. Wilson, R. M. Meneghini, and S. R. Anton, "Embedded piezoelectrics for sensing and energy harvesting in total knee replacement units," in *SPIE Smart Structures and Materials+ Nondestructive Evaluation and Health Monitoring*, 2015.

[20] S. M. Kurtz, O. K. Muratoglu, M. Evans, and A. A. Edidin, "Advances in the processing, sterilization, and crosslinking of ultra-high molecular weight polyethylene for total joint arthroplasty," *Biomaterials,* vol. 20, pp. 1659-1688, 1999.

[21] S. R. Anton and H. A. Sodano, "A review of power harvesting using piezoelectric materials (2003–2006)," *Smart materials and Structures,* vol. 16, p. R1, 2007.

[22] S. M. Kurtz, *UHMWPE Biomaterials Handbook.* Boston: Academic Press, 2009.

[23] https://www.americanpiezo.com.

[24] I. J. Harrington, "A bioengineering analysis of force actions at the knee in normal and pathological gait," *Biomedical Engineering,* vol. 11, pp. 167-172, 1976.

[25] K. R. Kaufman, K. N. An, W. J. Litchy, and E. Y. S. Chao, "Physiological prediction of muscle forces—I. Theoretical formulation," *Neuroscience,* vol. 40, pp. 781-792, 1991.

[26] S. L. Delp, F. C. Anderson, A. S. Arnold, P. Loan, A. Habib, C. T. John, *et al.*, "OpenSim: Open-Source Software to Create and Analyze Dynamic Simulations of Movement," *IEEE Transactions on Biomedical Engineering,* vol. 54, pp. 1940-1950, 2007.

[27] D. D'Lima, B. Fregly, and C. Colwell, "Implantable sensor technology: measuring bone and joint biomechanics of daily life in vivo," *Arthritis Research & Therapy,* vol. 15, p. 203, 2013.

[28] H. J. Lundberg, V. Ngai, and M. A. Wimmer, "Comparison of ISO Standard and TKR patient axial force profiles during the stance phase of gait," *Proceedings of the Institution of Mechanical Engineers, Part H: Journal of Engineering in Medicine,* vol. 226, pp. 227-234, 2012.

[29] S. M. Kurtz, *UHMWPE biomaterials handbook: ultra high molecular weight polyethylene in total joint replacement and medical devices*, 3 ed.: William Andrew, 2015.

[30] "IEEE Standard on Piezoelectricity," ed: IEEE, 1987.

[31] S. Zhao and A. Erturk, "Deterministic and band-limited stochastic energy harvesting from uniaxial excitation of a multilayer piezoelectric stack," *Sensors and Actuators A: Physical,* vol. 214, pp. 58-65, 2014.

[32] H. Chen, M. Liu, W. Hao, Y. Chen, C. Jia, C. Zhang, *et al.*, "Low-power circuits for the bidirectional wireless monitoring system of the orthopedic implants," *IEEE Transactions on Biomedical Circuits and Systems,* vol. 3, pp. 437-443, 2009.

[33] H. Chen, X. Zhang, M. Liu, W. Hao, C. Jia, H. Jiang, *et al.*, "Low-power circuits for the wireless ligament balance measurement system in TKA," *Analog Integrated Circuits and Signal Processing,* vol. 72, pp. 293-302, 2012.

[34] H. Kim, S. Priya, H. Stephanou, and K. Uchino, "Consideration of impedance matching techniques for efficient piezoelectric energy

harvesting," *IEEE transactions on ultrasonics, ferroelectrics, and frequency control,* vol. 54, pp. 1851-1859, 2007.

[35]   J. Feenstra, J. Granstrom, and H. Sodano, "Energy harvesting through a backpack employing a mechanically amplified piezoelectric stack," *Mechanical Systems and Signal Processing,* vol. 22, pp. 721-734, 2008.

[36]   M. G. Bautista, E. Dutkiewicz, and M. Heimlich, "Subthreshold energy harvesters circuits for biomedical implants applications," in *Proceedings of the 10th EAI International Conference on Body Area Networks*, 2015, pp. 127-131.

[37]   D. J. Krzypow and C. M. Rimnac, "Cyclic steady state stress–strain behavior of UHMW polyethylene," *Biomaterials,* vol. 21, pp. 2081-2087, 2000.

Mohsen Safaei was born in Isfahan, Iran in 1986. He received his B.S. from University of Yazd, Iran in 2008 and his M.S. in Mechanical Engineering from Isfahan University of Technology, Iran in 2011. He joined the Dynamic and Smart Systems Laboratory (DSSL) of Tennessee Technological University in 2015 to pursue his Ph.D. His current research interest includes the design of an instrumented knee implant.

R. Michael Meneghini is an Associate Professor of Orthopaedic Surgery at Indiana University School of Medicine and the Director of Orthopaedics and Joint Replacement at Indiana University Health Saxony Hospital. Dr. Meneghini graduated from Indiana University School of Medicine in 1999 and matriculated to Rush University College of Medicine for his Orthopaedic Surgery Residency. He then completed his fellowship in advanced hip and knee replacement at Mayo Clinic in Rochester, Minnesota and has been a practicing academic orthopaedic surgeon since 2005. He is the author of over 75 scientific articles on hip and knee replacement and is a member of the prestigious Hip and Knee Societies. Dr. Meneghini has won several awards, which include the Career Development Award from the Orthopaedic Research and Education Foundation and the prestigious Mark Coventry award for the outstanding fellow in Hip and Knee Adult Reconstruction at Mayo Clinic. Dr. Meneghini was most recently named in the "Top 22 Knee Surgeons in North America" by Orthopedics This Week and was awarded a Career Achievement Award in 2015 by his engineering undergraduate alma mater, Rose-Hulman Institute of Technology.

Steven R. Anton is an Assistant Professor of Mechanical Engineering at Tennessee Technological University. He is the director of the Dynamic and Smart Systems Laboratory (DSSL). He received his Ph.D. degree from Virginia Tech in 2011. Since 2007 he has published over 50 articles in refereed journals and conference proceedings on smart materials. He is an elected member of the ASME Adaptive Structure and Material Systems Branch and is a member of ASME and SPIE. His research interests include energy harvesting, self-powered biomedical sensing, structural health monitoring and damage detection, vibrations, and structural dynamics.

List of figures:

Fig. 1. Schematic of a total knee replacement implant.

Fig. 2. Schematic of (a) conceptual UHMW bearing with multiple embedded piezoelectric transducers and (b) simplified UHMW bearing investigated in this work with a single embedded piezoelectric transducer.

Fig. 3. Axial force profile developed in OpenSim for a 165.7 lb (75 kg) male who is 70.8 in (180 cm) tall under normal walking gait.

Fig. 4. Cross-sectional view of finite element model showing embedded piezoelectric and mesh detail.

Fig. 5. Transferred force to the embedded PZT transducer obtained from FE.

Fig. 6. Simulation results for uniaxially loaded embedded monolithic piezoelectric including (a) output voltage vs. gait cycle and (b) average output power vs. load resistance.

Fig. 7. (a) Variation of peak generated voltage from piezoelectric stack for different number of piezoelectric layers under 1.01 $M\Omega$ resistive load; (b) variation of optimal resistive load to obtain maximum average power and the peak generated voltage under optimum resistive load for various number of piezoelectric layers.

Fig. 8. Simulation results for uniaxially loaded embedded 40-layer piezoelectric stack including (a) output voltage vs. gait cycle and (b) average output power vs. load resistance.

Fig. 9. Fabricated bearing showing (a) inserted piezoelectric and (b) fully assembled bearing.

Fig. 10. Experimental compression test setup including (a) MTS 810 servo hydraulic load frame, (b) close-up view of prototype bearing inserted into compression fixturing.

Fig. 11. Comparison of load profile generated by OpenSim and achieved by MTS test frame.

Fig. 12. Generated voltage for uniaxially loaded embedded piezoelectric element in UHMW with 80 μm gap obtained from (a) simulation and (b) experiment.

Fig. 13. Comparison of force profile on the piezoelectric measured by PZT (experiment) and obtained from simulation.

Fig. 14. Voltage output data for 4 UHMW samples with embedded piezoelectric element.

List of tables:

TABLE I. Geometric and material properties of UHMW bearing and piezoelectric transducer ($\varepsilon_0 = 8.85 \text{x} 10^{-12}$ F/m).

TABLE II. Pocket depth of UHMW samples.